Effects of the nanoplasma on the energetics of Coulomb explosion of molecular clusters in ultraintense laser fields

Isidore Last and Joshua Jortner
School of Chemistry, Tel Aviv University, Ramat Aviv, 69978 Tel Aviv, Israel
(Received 6 July 2005; published 9 January 2006)

We report on theoretical and computational studies of electron and nuclear energies in the Coulomb explosion of $(D_2)_{n/2}$ clusters ($n=250-33\,000$, cluster radius $R_0=11$ Å-55 Å) coupled to ultraintense Gaussian laser fields (laser peak intensities $I_M=10^{15}-10^{18}$ W cm^{-2}, pulse widths $\tau=25-50$ fs, and frequency $\nu=0.35$ fs^{-1}). Molecular dynamics simulations were fit by semiempirical relations for the average $E_{\rm av}$ and maximal E_M ion energies and for their dependence on the cluster radius (R_0) and on the laser parameters. This revealed two kinds of Coulomb explosion domains separated by the border radius $R_0^{(\rm I)}$, which marks complete cluster outer ionization and which depends on I_M and τ, (i) the cluster vertical ionization (CVI) domain ($R_0<R_0^{(\rm I)}$), where $E_{\rm av}$, $E_M\propto R_0^2$ is independent of the laser parameters, (ii) the non-CVI domain ($R_0>R_0^{(\rm I)}$), which prevails at lower laser intensities over a broad region of cluster sizes (i.e., at $I_M=10^{15}$ W cm^{-2}, $R_0>R_0^{(\rm I)}=6.2$ Å for $\tau=25$ fs, and $R_0>R_0^{(\rm I)}=9.5$ Å for $\tau=50$ fs). The effects of the persistent nanoplasma on Coulomb explosion in the non-CVI domain are manifested by a distinct cluster size dependence, i.e., $E_{\rm av}\propto R_0^{\eta}$ ($\eta=0$) and $E_M\propto R_0^{\eta}$ ($\eta=1$) for $R_0>(2.0-2.5)R_0^{(\rm I)}$, and by a bimodal distribution of the ion kinetic energies. The energetics of Coulomb explosion in the non-CVI domain and its dependence (or independence) on the cluster size and laser parameters was semiquantitatively described by a cold nanoplasma model, which is based on a lychee configuration of the cluster charge, and which induces Coulomb explosion in the presence of the persistent nanoplasma. The results of our analyses are general for the cluster size dependence of the energetics of Coulomb explosion of multicharged elemental and molecular Xe_n, $(CH_4)_n$, and $(DI)_n$ clusters in the non-CVI domain.

DOI: 10.1103/PhysRevA.73.013202 PACS number(s): 36.40.Gk, 36.40.Qv, 36.40.Wa

I. INTRODUCTION

New developments in the experimental [1–15] and theoretical [16–30] exploration of the dynamics of large finite systems pertain to electron-nuclear dynamics of large molecules and clusters in ultraintense laser fields (laser peak intensities $I_M=10^{15}-10^{20}$ W cm^{-2}). This research area transcends femtosecond nuclear dynamics on the time scale of nuclear motion [31–34], unveiling features of attosecond/femtosecond electron dynamics [35,36], which triggers femtosecond nuclear dynamics [18,25–28]. The response of elemental [1–3,5,6,11,13,15], molecular [4,7,9,10,12–14] and metal [8,37,38] clusters to ultraintense laser fields manifests sequential-parallel processes of electron dynamics involving inner ionization, nanoplasma formation and outer ionization [6,16,24,28,36]. Nanoplasma response and ionization by the laser field is accompanied and followed by nuclear (ion) dynamics of Coulomb explosion [6,23,27] of extremely charged ions, e.g., H^+, D^+, $C^{q+}(q=4-6)$, $O^{q+}(q=6-8)$, $Xe^{q+}(q=3-36)$ [2,4,22,24,39,40]. Theoretical and computational studies of electron dynamics of clusters in ultraintense laser fields focused on extreme inner-outer ionization levels, as well as on time scales for nanoplasma formation, persistence and decay, while exploration of nuclear dynamics considered the ion energetics and the time scales of Coulomb explosion [6,16–30,36–40]. From these studies information emerged on the dependence of the energetic and dynamic observables for electrons and nuclei on the cluster size, and the dependence on the laser parameters (i.e., pulse shape, temporal width, and peak intensity). In particular, theoretical and computational studies of nuclear dynamics resulted in detailed information on the ion energy, i.e., maximal energies and ion energy distribution, and their dependence on the cluster size and on the laser pulse intensity [16–30,39,40].

Experimental data for electron dynamics in clusters, coupled to ultraintense laser fields, are scarce and are available only for electrons ejected from the cluster [3,41]. Information on energies of nanoplasma electrons within the clusters emerged from molecular dynamics simulations of high-energy electrons (with an average kinetic energy of $\epsilon=50-60$ eV at $I=10^{16}$ W cm^{-2} and $\epsilon\simeq 0.4-0.9$ keV at $I_M=10^{18}$ W cm^{-2} in the $(Xe)_n$ clusters [36]). The validity conditions for the applicability of classical molecular dynamics to the nanoplasma electrons rests on the conditions for the localization of the wave packet [42] and for the distinguishability of identical particles [43]. The wave packet localization condition [42] implies that the de Broglie wavelength $\lambda_{\rm DB}=h(2m\epsilon)^{-1/2}$ is considerably smaller than the interelectron separation $r_0=R_0/n^{1/3}\simeq 3.1$ Å [27], where R_0 is the initial deuterium cluster radius and n is the number of electrons. For $\epsilon=1$ keV, $\lambda_{\rm DB}=0.36$ Å, while for $\epsilon=100$ eV, $\lambda_{\rm DB}=1.1$ Å, whereupon the condition $\lambda_{\rm DB}<r_0$ is well satisfied for $\epsilon=1$ keV electrons (at $I_M\geqslant 10^{17}$ W cm^{-2} [22,36]), and is still valid for $\epsilon=100$ eV electrons (at $I_M\geqslant 10^{15}$ W cm^{-2} [22]). The distinguishability condition for identical particles, which implies the neglect of quantum permutation symmetry constraints, is valid provided that [43] $f=\exp[-(r_0/\lambda_{\rm DB})^2]\ll 1$. For $\epsilon=1$ keV, $f\simeq 10^{-32}$, while for $\epsilon=100$ eV, $f=4\times 10^{-4}$, so this condition is satisfied over the entire relevant electron energy domain.

Coulomb explosion in an assembly of $(D_2)_{n/2}$ clusters triggers nuclear fusion [7,14], whereupon the energetics of

 ©2006 The American Physical Society

the D^+ ions produced by the $(D^+)_n \rightarrow nD^+$ process is of interest. Our computational and theoretical studies of the cluster size dependence (characterized by the cluster radius R_0) of the average energies $E_{\rm av}$ and of the maximal energies E_M of deuterons produced by Coulomb explosion of $(D_2)_{n/2}$ clusters [22,27] established the cluster vertical ionization (CVI) domain, where $E_{\rm av}, E_M \propto R_0^2$ and the energy distribution $P(E) \propto E^{1/2}$, being independent on I_M [16,18,22,25,27]. The laser intensity and cluster size range for the prevalence of the CVI domain are characterized by the condition $R_0 \leqslant R_0^{(\rm I)}$, where $R_0^{(\rm I)}$ is the border cluster radius, which is characterized by complete outer ionization [27,28,40,44]. In the CVI domain, a quantitative agreement between the theoretical and the computational results for the ion energies was established [21,22,25,27,40]. At $R_0 > R_0^{(\rm I)}$ the energetics of Coulomb explosion manifests near saturation of $E_{\rm av}$ with increasing R_0. In the $(D_2)_{n/2}$ cluster size domain ($n=460-8000$) previously studied by the authors of this paper [27], these severe deviations from the CVI were manifested for $I_M = 10^{15}-10^{16}$ W cm^{-2}, an intensity domain of considerable experimental interest [2,6,9,12,13]. These deviations from the CVI scaling were documented for Coulomb explosion of deuterium homonuclear clusters [27] as well as for heteroclusters [28]. However, a quantitative description of the energetics in the non-CVI domain was not developed. In this paper we explore the energetics of Coulomb explosion of $(D_2)_{n/2}$ clusters ($n=250-33\,000$, $R_0=11$ Å-55 Å) in the range of the laser intensity, the laser pulse length and the cluster size, where the cluster outer ionization is incomplete, so that the CVI conditions break down [27]. The simulation results of electron and nuclear dynamics were fit by empirical relations for the $E_{\rm av}$ and E_M energies and for the energy distribution of the deuterons. In order to explain the features of Coulomb explosion in the non-CVI domain ($R_0 > R_0^{(\rm I)}$), we introduce a cold nanoplasma model for the occurrence of Coulomb explosion of clusters in the presence of the nanoplasma.

II. CLUSTER SIZE AND INTENSITY DEPENDENCE OF ION ENERGIES

The average and maximal atomic kinetic energies $E_{\rm av}$ and E_M, respectively, of D^+ (ion) nuclei from Coulomb explosion of $(D_2)_{n/2}$ clusters was determined from molecular dynamics simulations for the (high-energy) electrons and nuclei [40], in a cluster coupled to a Gaussian-shaped laser pulse,

$$I(t) = I_M \exp[-5.5(t/\tau)^2]\cos(2\pi\nu t). \quad (1)$$

The laser intensity $I(t)$ is assumed to be uniform inside a cluster. This assumption is valid, provided that the light wavelength λ is much larger than the cluster size and if the laser light is not noticeably attenuated by absorption while propagating through the cluster. For the laser frequency $\nu=0.35$ fs^{-1} [27,40], used in the present work, the wavelength $\lambda=8750$ Å is considerably larger than the maximal cluster diameter of $2R_0=110$ Å considered by us. The problem of the light attenuation will be further discussed below.

In the laser intensity range, which is of interest to us ($I_M \geqslant 10^{15}$ W cm^{-2}), the initial time $t=t_s$ for the onset of the simulations is taken at the laser intensity $I(t_s)$, which corresponds to complete one-electron barrier suppression ionization of all the atoms in the molecular cluster [40]. For $(D_2)_{n/2}$ clusters, typical values of this onset time are [40] $t_s=-9.7$ fs at $I_M=10^{15}$ W cm^{-2}, $t_s=-19$ fs at $I_M=10^{16}$ W cm^{-2}, $t_s=-24$ fs at $I_M=10^{17}$ W cm^{-2}, and $t_s=-29$ fs at $I_M=10^{18}$ W cm^{-2}. Thus, for deuterium clusters studied herein, the inner ionization is taken to be complete at $t=t_s$ [40] and we focus on the dynamics of the nanoplasma response, on the electron outer ionization dynamics, and on nuclear Coulomb explosion. For a lower intensity range ($I_M < 10^{15}$ W cm^{-2}) a complete description of inner ionization by barrier tunneling [24] will be required.

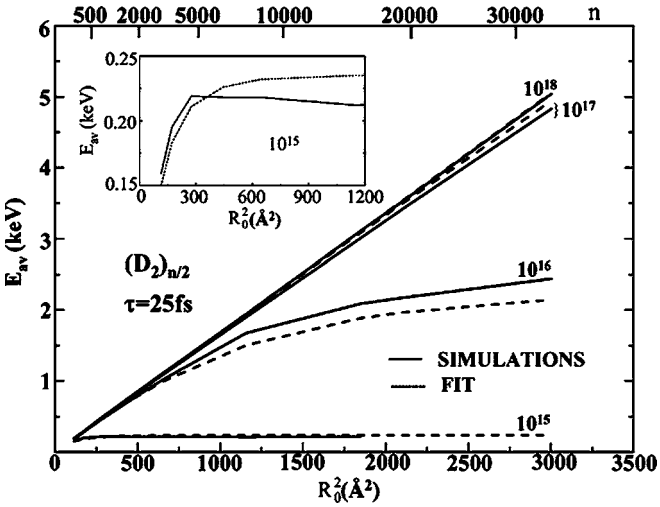

FIG. 1. Cluster size dependence of the average $E_{\rm av}$ energies of D^+ ions from Coulomb explosion of $(D_2)_{n/2}$ clusters induced by Gaussian pulses ($\tau=25$ fs) in the intensity range $I_M=10^{15}-10^{18}$ W cm^{-2}. The numbers 10^x, $x=15-18$, on the curves mark the intensities in units of W cm^{-2}. Data represented as $E_{\rm av}$ vs R_0^2. (—) Average energies obtained from simulations. (---) Average energies from the fitting equation, Eq. (6). The simulated and fitting data for $I_M=10^{18}$ W cm^{-2} are nearly indistinguishable, corresponding to the CVI limit. The inset represents the $E_{\rm av}$ vs R_0^2 dependence for $I_M=10^{15}$ W cm^{-2}, which exhibits saturation.

Most of the simulations reported in this section and analyzed in Secs. II and IV were performed with pulse widths of $\tau=25$ fs and $\tau=50$ fs. These results for the energetics with $\tau=25$ fs are portrayed in Figs. 1 and 2. Under CVI conditions the cluster size dependence of the average $E_{\rm av}$ and the maximal E_M energies is expected to obey the scaling law [27]

$$E_{\rm av} = (4\pi/5)\alpha \bar{B} q^2 \rho R_0^2 \quad (2)$$

and

$$E_M = 5E_{\rm av}/3, \quad (3)$$

where $\bar{B}=14.4$ eV Å, $q=1$ is the deuteron ionic charge, ρ is the cluster initial atomic density ($\rho=0.05$ Å^{-3} for deuterium clusters), and α is a numerical coefficient close to unity [27]. These features of Coulomb explosion energetics are well described by complete outer ionization [16,18,22,25,27]. The single cluster energy distribution is given by [27]

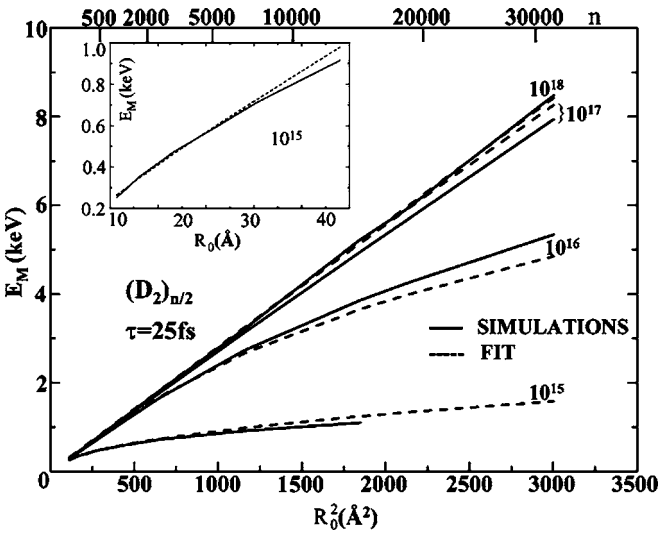

FIG. 2. Cluster size dependence of the maximal E_M energies of D^+ ions from Coulomb explosion of $(D_2)_{n/2}$ clusters induced by Gaussian pulses (τ=25 fs) in the intensity range $I_M=10^{15}-10^{18}$ W cm^{-2}. The numbers 10^x, $x=15-18$, on the curves mark the intensities in units of W cm^{-2}. Data in main panel represented as E_M vs R_0^2. (—) Maximal energies obtained from simulations. (---) Maximal energies from the fitting equation, Eq. (7). The simulated and fitting data for $I_M=10^{18}$ W cm^{-2} are nearly indistinguishable, corresponding to the CVI limit. The inset represents the E_M vs R_0 dependence for $I_M=10^{15}$ W cm^{-2}, which exhibits a near-linear relation.

$$P(E) = (3/2E_M)(E/E_M)^{1/2}, \quad E \leqslant E_M,$$
$$P(E) = 0, \quad E > E_M. \tag{4}$$

The CVI validity conditions and Eqs. (2)–(4) are applicable for the cluster size domain $R_0 < R_0^{(\mathrm{I})}$. This border radius is intensity (I_M) dependent and is expected to depend on other laser pulse parameters, e.g., the pulse duration. $R_0^{(\mathrm{I})}$ marks the upper limit of R_0 for complete depletion of the nanoplasma by outer ionization and manifests the onset of the breakdown of the CVI [27,28]. For $(D_2)_{n/2}$ clusters [in the laser field, Eq. (1), with τ=25 fs], we infer from an electrostatic model [27] that

$$R_0^{(\mathrm{I})} = 2.2 \times 10^{-7} I_M^{1/2} \tag{5}$$

with $R_0^{(\mathrm{I})}$/Å and I_M/W cm^{-2}. According to the simulation results (Figs. 1 and 2) the CVI scaling rules, Eqs. (2) and (3), are obeyed in the whole R_0 interval studied herein for strong laser intensities of $I_M \geqslant 10^{18}$ W cm^{-2}, where the CVI border radius, Eq. (5), is large, i.e., $R_0^{(\mathrm{I})} \geqslant 220$ Å. At lower intensities the border radius decreases, as manifested by the deviations from the CVI behavior, with the increase of E_{av} and E_M with R_0 being slowed down. A most striking feature of Coulomb explosion energetics is demonstrated for $I_M=10^{15}$ W cm^{-2} in the extreme domain of $R_0 \gg R_0^{(\mathrm{I})}$, presented in the insets of Figs. 1 and 2. In this lower intensity domain of $I=10^{15}$ W cm^{-2} [where $R_0^{(\mathrm{I})}=7$ Å, according to Eq. (5)], the average energy E_{av} dependence on R_0 exhibits saturation,

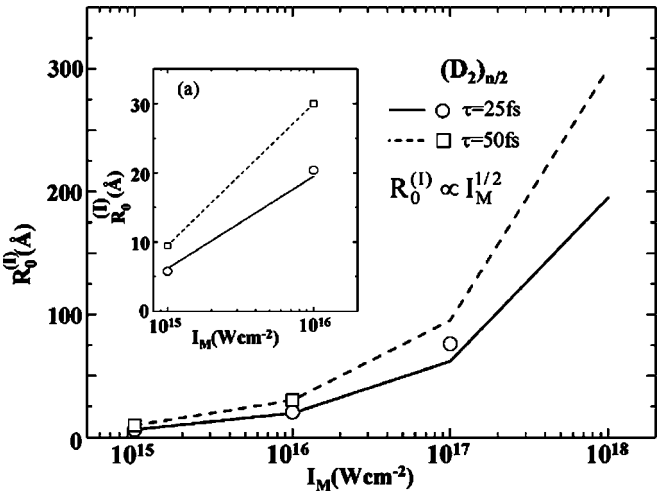

FIG. 3. The dependence of the border radius $R_0^{(\mathrm{I})}$ on the laser peak intensity I_M for laser pulse widths τ=25 fs and τ=50 fs. The dots represent simulated data. (○) τ=25 fs, (□) τ=50 fs as obtained for the complete depletion of the nanoplasma (see text). The curves, — (τ=25 fs) and --- (τ=50 fs) represent the $R_0^{(\mathrm{I})} \propto I_M^{1/2}$ scaling according to Eq. (8) (see text). The inset represents the $R_0^{(\mathrm{I})}$ vs I_M dependence in the lower intensity domain of $I_M=10^{15}-10^{16}$ W cm^{-2}.

while the maximal energy E_M continues to increase, roughly as $E_M \propto R_0$.

Over the entire intensity domain the simulation results for E_{av} and E_M can be well fit (Figs. 1 and 2) by the empirical relations

$$E_{\mathrm{av}}(I_M, R_0) = \alpha(4\pi/5)\bar{B}q^2\rho R_0^2[1 + (\beta R_0/R_0^{(\mathrm{I})})^4]^{-1/2} \tag{6}$$

and

$$E_M = \alpha(4\pi/3)\bar{B}q^2\rho R_0^2[1 + (\tilde{\beta} R_0/R_0^{(\mathrm{I})})^4]^{-1/4}, \tag{7}$$

where α=0.93, β=0.52, $\tilde{\beta}$=0.60, and $R_0^{(\mathrm{I})}$ is represented by the empirical relation

$$R_0^{(\mathrm{I})} = A I_M^{1/2} \tag{8}$$

with $A=1.95\times10^{-7}$ Å/(W cm^{-2})$^{1/2}$ for τ=25 fs. The border cluster radius $R_0^{(\mathrm{I})}$ obtained from the empirical relation, Eq. (8), is not markedly different from the theoretical value, Eq. (5), and from the estimates based on simulations for the complete depletion of the nanoplasma [27], the deviation being 10%–25% (Fig. 3).

Equations (6) and (7) provide fitting equations for E_{av} and E_M, which are approximately reduced to the $E_{\mathrm{av}}, E_M \propto R_0^2$ CVI limit, Eq. (2), at low intensities ($I_M < 10^{17}$ W cm^{-2}) and for low (intensity dependent) cluster sizes, while at high intensities ($I_M > 10^{17}$ W cm^{-2}) the CVI limit is applicable over the entire cluster size domain studied herein. The simulation results of Fig. 1, which are in good agreement with Eq. (6), mark the CVI atomic energy scaling region ($R_0 < R_0^{(\mathrm{I})}$), the onset of the slowing down of the average atomic energy increase with increasing R_0 ($\simeq R_0^{(\mathrm{I})}$), and the saturation of the average atomic energy at $R_0 \gg R_0^{(\mathrm{I})}$. The

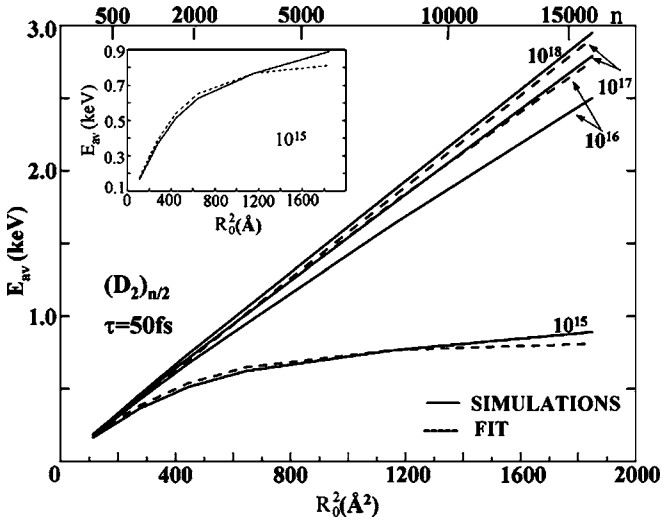

FIG. 4. Cluster size dependence of the average E_{av} energies of D^+ ions from Coulomb explosion of $(D_2)_{n/2}$ clusters induced by Gaussian pulses (τ=50 fs) in the intensity range $I_M=10^{15}-10^{18}$ W cm^{-2}. The numbers 10^x, x=15–18, on the curves mark the intensities in units of W cm^{-2}. Presentation of data as in Fig. 1. (—) Average energies obtained from the simulations. (---) Average energies obtained from the fitting equation, Eq. (6). The inset represents the E_{av} vs R_0^2 dependence for $I_M=10^{15}$ W cm^{-2}, which exhibits near saturation at considerably larger E_{av} values than for τ=25 fs (inset to Fig. 1).

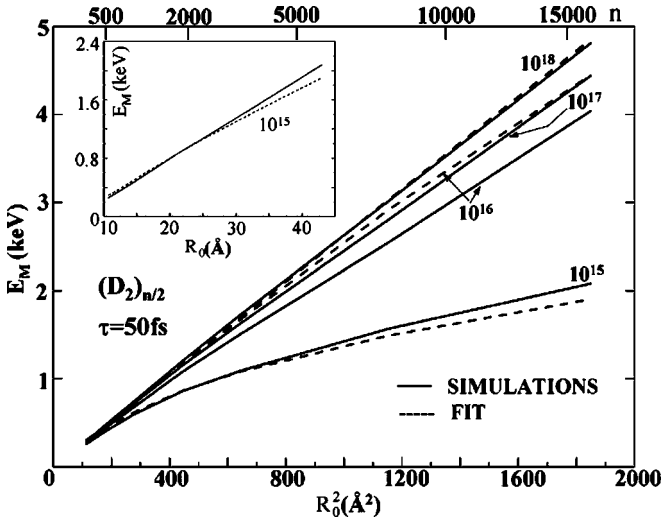

FIG. 5. Cluster size dependence of the maximal E_M energies of D^+ ions (deuterons) from Coulomb explosion of $(D_2)_{n/2}$ clusters induced by Gaussian pulses (τ=50 fs) in the intensity range $I_M=10^{15}-10^{18}$ W cm^{-2}. The numbers 10^x, x=10–18, on the curves mark the intensities in units of W cm^{-2}. (—) Maximal energies obtained from the simulations. (---) Maximal energies obtained from the fitting equation, Eq. (7). The inset represents the E_M vs R_0 dependence for $I_M=10^{15}$ W cm^{-2}, which exhibits a linear dependence with considerably larger E_M values than for τ=25 fs (inset to Fig. 2).

fitting equation for the maximal energy E_M, Eq. (7), coincides with the CVI result, Eq. (3), for $R_0<R_0^{(I)}$ (Fig. 2). In the non-CVI domain of $R_0>R_0^{(I)}$, Eq. (7) fits the roughly linear increase of E_M with increasing R_0 (Fig. 2). While in the CVI range ($R_0<R_0^{(I)}$) the cluster size dependence of both E_{av} and of E_M is identical, in accordance with Eqs. (2) and (3), the dependence of E_{av} and E_M on R_0 is quantitatively different in the non-CVI ($R_0>R_0^{(I)}$) range. This interesting feature of the non-CVI domain reflects on the Coulomb explosion dynamics of a charged cluster in the presence of the nanoplasma (Sec. III).

The energetic data for E_{av} and E_M (Figs. 1 and 2), together with the $R_0^{(I)}$ data (Fig. 3), were obtained for the laser pulse width of τ=25 fs. As recently shown in Ref. [27] the increase of the Gaussian pulse width affects the energetics of the D^+ ions. To obtain some additional information on the dependence of these data on the laser pulse parameters, we performed simulations for E_{av} and E_M induced by a laser pulse of τ=50 fs (Figs. 4 and 5). At the higher laser intensities of $I_M\geqslant 10^{17}$ W cm^{-2}, the E_{av} and E_M energies for the longer τ=50 fs pulse (Figs. 4 and 5) manifest the CVI behavior, Eqs. (2) and (3), as in the case of the τ=25 fs pulse (Figs. 1 and 2). The E_{av} and E_M data obtained for τ=50 fs are only slightly lower (by ~6%) than the corresponding data for the τ=25 fs pulse, so that the effect of the laser pulse length on the energetics in the CVI region is only minor.

For a pulse length of τ=50 fs, the CVI relation for E_{av} and for E_M breaks down for intensities of $I_M=10^{15}-10^{16}$ W cm^{-2} (Figs. 4 and 5) and E_{av} vs R_0^2 exhibits near saturation, e.g., for $I=10^{15}$ W cm^{-2} at the largest value of R_0=43 Å studied herein (Fig. 4). This trend for E_{av} at τ=50 fs is qualitatively similar to the one observed for the shorter τ=25 fs pulse (Fig. 1). Most important, the near-saturation value of E_{av} is considerably larger for τ=50 fs than for τ=25 fs at a fixed I_M ($10^{15}-10^{16}$ W cm^{-2}) in the non-CVI regime (inserts to Figs. 4 and 5). The CVI border radii $R_0^{(I)}$ may be found by the outer ionization criterion, with $R_0^{(I)}$ being equal to the initial radius R_0 of a cluster whose outer ionization process is completed at the intensity peak t=0 [27]. It was suggested [36] that the outer ionization is completed when 95% of the electrons are removed from the cluster. Using the outer ionization criterion for the τ=50 fs simulation resulted in $R_0^{(I)}$=9.5 Å and 30 Å for $I_M=10^{15}$ W cm^{-2} and 10^{16} W cm^{-2}, respectively. For $I_M\geqslant 10^{17}$ W cm^{-2}, $R_0^{(I)}$ cannot be directly determined in the cluster size domains considered by us, $R_0\leqslant$43 Å (Fig. 4), as the outer ionization at these intensities is completed at $t<0$ before the laser pulse peak. The two $R_0^{(I)}$ radii obtained by us for the laser intensity interval $I_M=10^{15}-10^{16}$ W cm^{-2} fit the scaling rule, Eq. (8), $R_0^{(I)}\propto I_M^{1/2}$, with $A=3.0\times10^{-7}$ Å/(W cm^{-2})$^{1/2}$ at τ=50 fs. This $R_0^{(I)}$ dependence on I_M was extended to the entire I_M domain (Fig. 3). The simulated E_{av} energies for τ=50 fs could be fit by Eq. (6) with the $R_0^{(I)}$ radii of Eq. (8) and with the empirical parameters α=0.87 and β=0.41 (Fig. 4), instead of the value β=0.52 for τ=25 fs.

The cluster size dependence of the E_M energies for τ=50 fs at $I_M=10^{15}-10^{16}$ W cm^{-2} (Fig. 5) manifests large deviations from the CVI, with an increase of E_M vs R_0 over the entire R_0 domain, being qualitatively similar to the pattern for τ=25 fs. However, the E_M values for τ=50 fs are

systematically larger than the corresponding data for $\tau=25$ fs (insets to Figs. 2 and 5). The simulated E_M energies for $\tau=50$ fs could be empirically fit (Fig. 5) by Eq. (7) with the parameter $\tilde{\beta}=0.56$ (instead of $\tilde{\beta}=0.60$ for $\tau=25$ fs), and using the $R_0^{(I)}$ values from Eq. (8).

Our simulations provide the energy E_{abs}, which is absorbed by the cluster, per laser pulse. E_{abs} will be compared with the laser energy flow E_f through the cluster. Neglecting the cluster expansion due to Coulomb explosion, we present the energy flow as $E_f=\pi R_0^2\int_{-\infty}^{\infty}I(t)dt$. From the comparison between E_f and E_{abs} we shall be able to establish whether light absorption significantly contributes to the attenuation of the laser intensity within a single cluster and, consequently, to the violation of the uniformity of the intensity, which is implied by Eq. (1). Due to energy balance, E_{abs} is equal to the final total energy of all the particles, i.e., ions and electrons. On the basis of our simulations $E_{abs}\propto R_0^{\eta}$, where $\eta=3$ in the non-CVI domain and $\eta=5$ in the CVI domain. On the other hand, $E_f\propto R_0^2$. As $E_{abs}/E_f\propto R_0^{\eta-2}$, the contribution of light absorption increases with increasing the cluster size. The largest clusters employed in our simulations correspond to $R_0=43$ Å at $I_M=10^{15}$ W cm^{-2} and $R_0=55$ Å at $I_M\geqslant 10^{16}$ W cm^{-2}. For these cluster sizes (for a laser pulse width of $\tau=25$ fs), the following energetic data were obtained, $E_{abs}=3.3\times10^6$ eV and $E_f=3.4\times10^7$ eV at $I=10^{15}$ W cm^{-2}, $E_{abs}=8.1\times10^7$ eV and $E_f=5.5\times10^8$ eV at $I=10^{16}$ W cm^{-2}, $E_{abs}=1.6\times10^8$ eV and $E_f=5.5\times10^9$ eV at $I=10^{17}$ W cm^{-2}, while $E_{abs}=1.7\times10^8$ eV and $E_f=5.5\times10^{10}$ eV at $I=10^{18}$ W cm^{-2}. In the non-CVI domain ($I_M=10^{15}-10^{16}$ W cm^{-2}), $E_{abs}/E_f\simeq0.1$, while in the CVI regime ($I_M\geqslant10^{17}$ W cm^{-2}) $E_{abs}/E_f<0.03$. The small contribution of laser absorption for deuterium clusters justifies the neglect of the attenuation of the light intensity inside a cluster and insures the validity of Eq. (1).

From the analyses of the simulation results (Figs. 1, 2, 4, and 5) for the dependence of E_{av} and E_M on the laser pulse length we conclude the following:

(1) The CVI relations for the energetics at the highest intensities of $I_M>10^{17}$ W cm^{-2} are nearly independent of the laser pulse parameters τ and I_M.

(2) In the non-CVI intensity domain of $I_M=10^{15}-10^{16}$ W cm^{-2}, the E_{av} and E_M energies can be well fit (within an accuracy of 15%) by the empirical relations, Eqs. (6) and (7), with the border radii $R_0^{(I)}$ manifesting a τ dependence, which will be discussed in point (4) below.

(3) In the non-CVI intensity domain of $I_M=10^{15}-10^{16}$ W cm^{-2}, the values of E_{av} and E_M for a fixed cluster size markedly increase with increasing the pulse length (insets to Figs. 1, 2, 4, and 5).

(4) The border radii $R_0^{(I)}$, at fixed I_M, exhibit a marked increase with increasing the pulse length. For $I_M=10^{15}$ W cm^{-2}, $R_0^{(I)}=9.5$ Å for $\tau=50$ fs, while $R_0^{(I)}=6.2$ Å for $\tau=25$ fs. For $I_M=10^{16}$ W cm^{-2}, $R_0^{(I)}=30$ Å for $\tau=50$ fs, while $R_0^{(I)}=19.5$ Å for $\tau=25$ fs. These results can be fit for a Gaussian pulse by the relation $R_0^{(I)}=\tilde{A}I_M^{1/2}\tau^{\xi}$, with $\tilde{A}=2.65\times10^{-8}$ and $\xi=0.62$.

(5) The two values of $R_0^{(I)}$ for $\tau=50$ fs at $I_M=10^{15}$ W cm^{-2} and at $I_M=10^{16}$ W cm^{-2}, scale with the intensity as $R_0^{(I)}\propto I_M^{1/2}$, in accordance with the electrostatic model, Eq. (5).

The most interesting result of the present analysis involves the characterization of the non-CVI region, which exhibits a marked enhancement of the energetics of Coulomb explosion with increasing the laser pulse length [point (3) above]. This issue, which is related to the τ dependence of the border radius $R_0^{(I)}$ [point (4) above] pertains to Coulomb explosion of an incompletely ionized cluster in the presence of the nanoplasma.

III. THE COLD NANOPLASMA MODEL FOR THE NON-CVI DOMAIN

The Coulomb explosion features in the CVI domain ($R_0<R_0^{(I)}$) are well described by the model, which considers the cluster at the onset of Coulomb explosion as a purely ionic system (complete outer ionization) in the geometry of a neutral cluster [16,22,27]. In the opposite, non-CVI domain, case ($R_0>R_0^{(I)}$) the laser field is not sufficiently strong to remove all the electrons from the cluster. Then the outer ionization process occurs on a time scale comparable to the pulse duration [36], and the outer ionization level n_{oi} (determined as the number of electrons removed from the cluster per atom) becomes considerably lower than the inner ionization level n_{ii} ($n_{ii}=1$ for deuterium clusters) [40].

The ionization in the non-CVI ($R_0>R_0^{(I)}$) domain corresponds to the weak outer cluster ionization, whereupon Coulomb explosion occurs from the ionic cluster which still contains the nanoplasma. Simulations performed in the non-CVI domain, $R_0\gg R_0^{(I)}$, show that the nanoplasma electrons are not considerably heated by the laser radiation, most probably because of efficient energy acquisition of electrons removed from the cluster by the outer ionization process. This picture of high-energy emerging electrons and of low-energy remaining nanoplasma electrons bears analogy to cluster evaporative cooling. For example, in the D_{3367} cluster ($R_0=25.4$ Å) subjected to $I_M=10^{15}$ W cm^{-2} radiation ($R_0^{(I)}=6.2$ Å), the average kinetic energy of electrons at the pulse peak is $\sim$50 eV–100 eV, whereas the electron potential energy at the cluster borderline is about 550 eV. Accordingly, it is appropriate to refer to the nanoplasma as a (relatively) low-electron energy, "cold" nanoplasma.

Neglecting the electron kinetic energy we treat the cluster electrons as a "cold" nanoplasma, which forms a neutral sphere with a radius

$$R_p=(1-n_{oi})^{1/3}R, \tag{9a}$$

where R is the cluster radius and n_{oi} is the outer ionization level per D atom. The "cold" nanoplasma model involves a lychee configuration for the spatial distribution of the charge, with the ions from the electron-free spatial exterior range $R_p\leqslant r\leqslant R_0$ undergoing Coulomb explosion, while ions from the interior range $0\leqslant r\leqslant R_p$ of the neutral nanoplasma are characterized by low kinetic energy. The lychee configuration is expected to be valid at the lower intensity range of the ultraintense region, i.e., $I_M\sim10^{15}$ W cm^{-2}, where the nanoplasma interior and the ionic exterior are concentric. On the

basis of molecular dynamics electron-nuclei simulations for Xe_n clusters [36], such a central structure prevails for intensities of $I_M=10^{15}$ W cm^{-2}, while for intensities of $I_M=10^{16}$ W cm^{-2} the interior nanoplasma sphere is shifted from the cluster center [36], manifesting the onset of the breakdown of the cold nanoplasma model. The cluster expansion was found to be slow on the time scale of the evolution of the laser pulse, so that at the laser pulse peak, where the outer ionization process is most effective, $R/R_0 \simeq 1.10$, where R_0 is the initial radius. Ignoring this small radius increase we take $R=R_0$ in Eq. (9a). The simulations give $n_{oi}<0.4$ and, according to Eq. (9a), $(R_0-R_p)<0.16R_0$. Taking $s=R_0-R_p \ll R_0$, we estimate from Eq. (9a) that

$$n_{oi}=3s/R_0<1. \tag{9b}$$

At the cluster periphery, between R_p and R_0, a narrow charged shell consisting of only ions is formed. A simple electrostatic treatment provides the following expressions for the ion energetics:

$$E_{\mathrm{av}}=6\pi\bar{B}\rho s^2 \tag{10}$$

and

$$E_M=4\pi\bar{B}\rho s R_0, \tag{11a}$$

Eq. (11a) can be expressed in the alternative form

$$E_M=(10/3)^{1/2}(E_{\mathrm{av}}^{\mathrm{CVI}}E_{\mathrm{av}})^{1/2}, \tag{11b}$$

where $E_{\mathrm{av}}^{\mathrm{CVI}}=(4\pi/5)B\rho R_0^2$ is the CVI average energy, Eq. (2), for $\alpha=1$ and $q=1$, and E_{av} is given by Eq. (10), resulting in the relation $E_M^2/E_{\mathrm{av}} \propto E_{\mathrm{av}}^{\mathrm{CVI}}$.

Two conclusions emerge for the energetics of the "cold" nanoplasma model, Eqs. (10), (11a), and (11b), as follows:

(1) Independence of E_{av} on the cluster size (at fixed I_M and τ). Provided that s is independent of R_0, as will subsequently be demonstrated by the cluster barrier suppression ionization model [40], then E_{av} vs R_0^2 will exhibit saturation.

(2) Increase of E_M with increasing the cluster size (at fixed I_M and τ). Equation (11b) indicates that for a constant (saturated) average energy range of E_{av} the maximal ion energy E_M increases linearly with increasing the cluster radius R_0.

Conclusions (1) and (2) are in accordance with the simulation results (Figs. 1, 2, 4, and 5). In order to estimate the radius R_p of the neutral nanoplasma, we shall apply the cluster barrier suppression ionization (CBSI) model [40]. According to this model the total cluster ionic charge $Q_{\mathrm{cl}}=nn_{oi}$, with n being the number of atoms, is proportional to the laser field peak amplitude F_M, being given by

$$nn_{oi}=R_0^2eF_M/\sqrt{2}\bar{B}. \tag{12}$$

Also, the CVI border radius $R_0^{(\mathrm{I})}$ provided by the CBSI model is proportional to F_M [27]

$$R_0^{(\mathrm{I})}=eF_M\Big/\left(\frac{4\sqrt{2}\pi}{3}\bar{B}\rho\right). \tag{13}$$

Using Eqs. (13) and (9b) we obtain

$$s=R_0^{(\mathrm{I})}/3 \tag{14}$$

providing a relation between the width of the charged shell and the border radius. Two important features of the "cold" nanoplasma model emerge from Eq. (14). First, the width of the charged shell does not depend on the cluster radius. This result provides justification for the saturation of E_{av} in the non-CVI "cold" nanoplasma domain [point (1) above]. Second, due to the $R_0 \gg R_0^{(\mathrm{I})}$ condition, this shell is narrow, in accordance with the inequality condition in Eq. (9b).

To provide explicit relations for the energetics in the non-CVI, "cold" nanoplasma domain within the framework of the CBSI model, we establish the dependence of E_{av} and E_M on $R_0^{(\mathrm{I})}$. Substituting Eq. (14) into Eqs. (10) and (11) we find that

$$E_{\mathrm{av}}=(2\pi/3)\bar{B}\rho(R_0^{(\mathrm{I})})^2, \tag{15}$$

$$E_M=(4\pi/3)\bar{B}\rho R_0^{(\mathrm{I})}R_0, \tag{16}$$

while the ratio of the energies assumes the simple form

$$E_M/E_{\mathrm{av}}=2R_0/R_0^{(\mathrm{I})}. \tag{17}$$

Equations. (15)–(17) imply that for fixed laser parameters (I_M and τ) E_{av} is independent of the cluster radius [point (1) above], while $E_M \propto R_0$ [point (2) above], in accordance with the simulation results. Equations (15)–(17) account for the dependence of the energetics on the cluster size (or the lack of it) and on the laser parameters in the "cold" nanoplasma domain. In particular, these results properly account for the dependence of the energetics on the laser pulse length, which is attributed to the dependence of $R_0^{(\mathrm{I})}$ on τ (Sec. II). Thus for $I=10^{15}$ W cm^{-2} we expect that the enhancement of the average energy in the saturation region will be $E_{\mathrm{av}}(\tau=50\ \mathrm{fs})/E_{\mathrm{av}}(\tau=25\ \mathrm{fs})=[R_0^{(\mathrm{I})}(\tau=50\ \mathrm{fs})/R_0^{(\mathrm{I})}(\tau=25\ \mathrm{fs})]^2=2.4$, in accordance with the simulation data of Figs. 1 and 4, which give $E_{\mathrm{av}}(\tau=50\ \mathrm{fs})/E_{\mathrm{av}}(\tau=25\ \mathrm{fs})=4.0$, which is independent of R_0. For a fixed value of R_0 we expect that in the linear region of E_M vs R_0 we have $E_M(\tau=50\ \mathrm{fs})/E_M(\tau=25\ \mathrm{fs})=R_0^{(\mathrm{I})}(\tau=50\ \mathrm{fs})/R_0^{(\mathrm{I})}(\tau=25\ \mathrm{fs})=1.5$, in agreement with the simulation results of Figs. 2 and 5, which give $E_M(\tau=50\ \mathrm{fs})/E_M(\tau=25\ \mathrm{fs})=1.7$.

The "cold" nanoplasma model semiquantitatively accounts for the dependence of the energetics of Coulomb explosion on the temporal pulse width τ (Sec. II). To obtain a unified plot for the cluster size dependence of the energies, we utilize Eqs. (2), (3), (15), and (16) to obtain

$$E_{\mathrm{av}}^{\mathrm{CVI}}(R_0)/E_{\mathrm{av}}(R_0,I_M\tau)=(6/5)(R_0/R_0^{(\mathrm{I})})^2, \tag{18}$$

$$E_M^{\mathrm{CVI}}(R_0)/E_M(R_0,I_M,\tau)=(R_0/R_0^{(\mathrm{I})}), \tag{19}$$

where $E_{\mathrm{av}}(R_0,I_M,\tau)$ and $E_M(R_0,I_M,\tau)$ are the non-CVI energies, which depend on R_0, I_M, and τ, while $E_{\mathrm{av}}^{\mathrm{CVI}}(R_0)$ and $E_M^{\mathrm{CVI}}(R_0)$ are the corresponding CVI energies, Eqs. (2) and (3), which depend only on R_0. The energy ratios in Eqs. (18) and (19) depend on the ratios of the cluster radius and of the border radius, with the latter being dependent on I_M and τ. In Fig. 6 we present the unified plots of the energy ratios vs

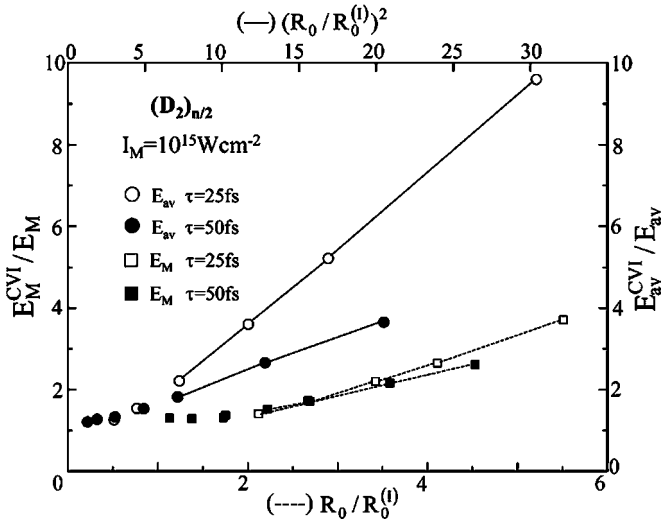

FIG. 6. The ratios of $E_{\mathrm{av}}^{\mathrm{CVI}}/E_{\mathrm{av}}$ vs $(R_0/R_0^{(\mathrm{I})})^2$ and of E_M^{CVI}/E_M vs $R_0R_0^{\mathrm{I}}$. $E_{\mathrm{av}}^{\mathrm{CVI}}$, Eq. (2), and E_M^{CVI}, Eq. (3), are the average and maximal energies in the CVI limit, respectively. Data at $I_M=10^{15}$ W cm^{-2} with $\tau=25$ fs and 50 fs. The points marked in the figure were obtained from simulations of E_{av} and of E_M. The energy ratios approach unity in the CVI domain for $R_0\leqslant R_0^{(\mathrm{I})}$. In the non-CVI domain, the "cold" nanoplasma model, Eqs. (18) and (19), predicts that these plots are linear, being marked by solid lines for the average energy ratios and by dashed lines for the maximal energy ratios.

$(R_0/R_0^{(\mathrm{I})})^2$ for E_{av} and vs $(R_0/R_0^{(\mathrm{I})})$ for E_M at $I_M=10^{15}$ W cm^{-2}, with the $R_0^{(\mathrm{I})}$ values increasing with increasing τ (Sec. II). In the CVI domain $(R_0<R_0^{(\mathrm{I})})$ these energy ratios assume values near unity. The increase of $R_0/R_0^{(\mathrm{I})}$ to values larger than unity marks the non-CVI domain. Linear plots of $E_{\mathrm{av}}^{\mathrm{CVI}}/E_{\mathrm{av}}$ vs $(R_0/R_0^{(\mathrm{I})})^2$ and of E_M^{CVI}/E_M vs $R_0/R_0^{(\mathrm{I})}$ are exhibited in the non-CVI domain (Fig. 6), as expected from Eqs. (18) and (19). However, the slopes of these linear plots for $E_{\mathrm{av}}^{\mathrm{CVI}}/E_{\mathrm{av}}$ and for E_M^{CVI}/E_M (Fig. 6) depend on τ, in contrast to the predictions of Eqs. (18) and (19), reflecting on the limitations of the model, which will be discussed below. From the linear portions of the energetic data in Fig. 6 we assert that the onset of the applicability of the non-CVI "cold" nanoplasma domain is manifested in the cluster size domain of $R_0=(2-2.5)R_0^{(\mathrm{I})}$.

From the foregoing analysis it is apparent that the E_{av} and E_M energies in the non-CVI "cold" nanoplasma domain are qualitatively described by the "cold" nanoplasma model. As will be shown in Sec. IV, this model also properly describes the shape of the kinetic energy distribution of the D^+ ions. The quantitative predictions of the "cold" nanoplasma model are less satisfactory. The non-CVI "cold" nanoplasma average energy E_{av}, Eq. (6), and the maximal energy E_M, Eq. (7), are

$$E_{\mathrm{av}}=(4\pi\alpha/5\beta^2)\bar{B}\rho(R_0^{(\mathrm{I})})^2, \tag{20a}$$

and

$$E_M=(4\pi\alpha/3\tilde{\beta})\bar{B}\rho R_0^{(\mathrm{I})}R_0. \tag{21a}$$

Substituting Eq. (8) into Eqs. (20a) and (21a), we obtain the intensity dependence of the energetics for

$$E_{\mathrm{av}}=(4\pi\alpha/5\beta^2)A^2\bar{B}\rho I_M, \tag{20b}$$

and

$$E_M=(4\pi\alpha/3\tilde{\beta})A\bar{B}\rho I_M^{1/2}R_0 \tag{21b}$$

with $E_{\mathrm{av}}\propto I_M$ being independent of R_0, while $E_M\propto I_M^{1/2}R_0$. The fitting equations (20a) and (21a), which quantitatively account for the simulation data, properly describe the dependence of the energies on $R_0^{(\mathrm{I})}$ and on R_0 in Eqs. (15) and (16), respectively. However, the proportionality coefficients in Eqs. (15) and (16) differ from those characterizing the exact simulation results, which appear in Eqs. (20a) and (21a), respectively. The proportionality parameter for $E_M(4\pi\alpha/3\tilde{\beta})$ in the fitting result in Eq. (21a) is larger by 47% (for $\tau=25$ fs) and by 59% (for $\tau=50$ fs) than the coefficient $(4\pi/3)$ in the model result, Eq. (16). As the contribution of the range $r\simeq R_0$ to E_M is dominating, the agreement between Eqs. (16) and (21a) is adequate. The discrepancy is larger for the E_{av} coefficient, which is $(4\pi\alpha/5\beta^2)$ for the fitting result, Eq. (21a), and $(2\pi/3)$ for the model result, Eq. (15), with differences of a numerical factor of 4 (for $\tau=25$ fs) and 6 (for $\tau=50$ fs) between the two coefficients. Using the numerical fits of the simulation data we expect from Eqs. (20a) and (21a) that $E_{\mathrm{av}}^{\mathrm{CVI}}/E_{\mathrm{av}}=\beta^2(R_0/R_0^{(\mathrm{I})})^2$ and $E_M^{\mathrm{CVI}}/E_M=\tilde{\beta}R_0/R_0^{(\mathrm{I})}$. The dependence of the β, $\tilde{\beta}$, and τ parameters accounts for the deviations from the "cold" nanoplasma model. This model is expected to underestimate the average kinetic energy of the ions, since the lychee picture for the spatial charge distribution implies that Coulomb explosion occurs only from the range $R_p\leqslant r\leqslant R_0$. However, the contribution of a low-energy component in the ion kinetic energy distribution originating from the spatial range $r\leqslant R_p$ is disregarded. This low-energy component is approximated by a delta function contribution within the "cold" nanoplasma model (Sec. IV), while in real life it is finite, making a large contribution to E_{av}. On the other hand, there is no contribution of this low-energy component to E_M.

IV. ENERGY DISTRIBUTION OF D^+ IONS IN COULOMB EXPLOSION

In the CVI domain, $R_0\leqslant R_0^{(\mathrm{I})}$, the energy distribution, Fig. 7(a), is well described by the $P(E)\propto E^{1/2}$ dependence, Eq. (4) [27]. In the opposite, non-CVI, domain of $R_0>R_0^{(\mathrm{I})}$ [Fig. 7(c)], the energy distribution is bimodal, consisting of a broad maximum located in the vicinity of zero energy and a high-energy tail. Such energy distribution is in qualitative agreement with the energy distribution of the "cold" nanoplasma model. In the framework of this model the ions located inside the neutral plasma (at $r<R_p$) are not subjected to Coulomb explosion and their kinetic energy is zero. The energy distribution of these ions is described by a delta function. Ions with nonzero energy are produced in the charged outer shell $R_p\leqslant r\leqslant R_0$. The product ion energy distribution is presented by the sum

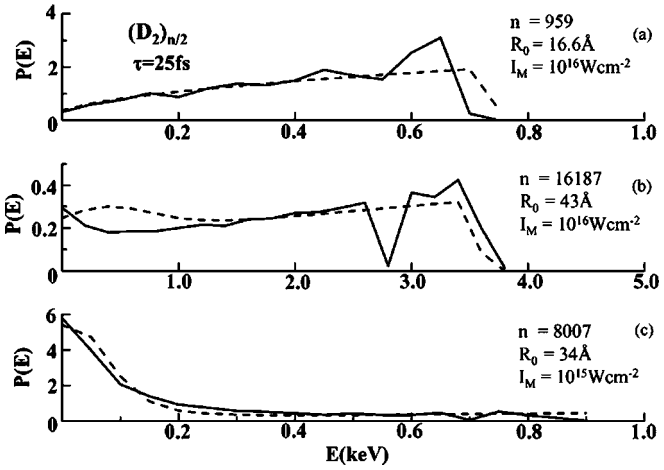

FIG. 7. Energy distributions $P(E)$ of D^+ ions from Coulomb explosion of $(D_2)_{n/2}$ clusters induced by the laser pulse with a temporal width of τ=25 fs. The solid lines represent simulation results and the dashed lines represent the fitting equation, Eq. (23). Cluster sizes and laser peak intensities are marked on the panels. (a) $P(E)$ in the CVI domain, (b) $P(E)$ in the intermediate domain, (c) $P(E)$ in the "cold" nanoplasma domain.

$$P(E) = (1 - n_{oi})\,\delta(E) + n_{oi}P_s(E), \tag{22a}$$

where $P_s(E)$ is the energy distribution of the ions from the charged shell. The electrostatic treatment of $P_s(E)$, applied together with Eqs. (9b) and (11a) for R_0-$R_p \ll R_0$, gives

$$P(E) = (1 - n_{oi})\,\delta(E) + (n_{oi}/E_M)\left[1 + \frac{1}{3}n_{oi}\left(2\frac{E}{E_M} - 1\right)\right]. \tag{22b}$$

The bimodal distribution, Eq. (22b), provides a qualitative description of the simulation data (Fig. 7). In the real cluster, the low-energy deuterons are described by a finite size maximum in the energy distribution, instead of by a δ function, as in Eq. (22b). This low-energy maximum includes the majority of the cluster deuterons. The high-energy tail demonstrates a slight increase of $P(E)$, with E increasing up to the vicinity of the maximal energy E_M, in accordance with the $P_s(E)$ component in Eqs. (22a) and (22b). In the intermediate case, when $R_0 \simeq 2R_0^{(I)}$ [Fig. 7(b)], the low-energy maximum is small and the high-energy tail resembles approximately the CVI energy distribution, Eq. (4).

In order to properly describe the energy distribution for any cluster size, we suggest, in analogy with Eqs. (22a) and (22b), to use a two-component fitting equation for the bimodal distribution

$$P(E) = C_1P_1(E) + (1 - C_1)P_2(E), \tag{23}$$

where $P_1(E)$ is the low-energy component and $P_2(E)$ is the CVI energy distribution, Eq. (4), with the maximal energy E_M, Eq. (7). Trying different functions to fit the simulation energy distributions we choose the form

$$P_1(E) = (4\sqrt{2}/\pi E_{\rm av})/[1 + (2E/E_{\rm av})^4]. \tag{24}$$

The energy distribution presented by Eq. (23) yields the average energy

$$\widetilde{E}_{\rm av} = \int_0^{E_M} EP(E)dE \tag{25}$$

which must be equal to the average energy $E_{\rm av}$ in Eq. (6). Using Eqs. (4), (24), and (25) to calculate $\widetilde{E}_{\rm av}$, we utilized the condition $\widetilde{E}_{\rm av}$=$E_{\rm av}$ to evaluate the coefficient C_1 in Eq. (23),

$$C_1 = \left(\frac{3}{5}E_M - E_{\rm av}\right) \Big/ \left(\frac{3}{5}E_M - \frac{1}{2\sqrt{2}}E_{\rm av}\right). \tag{26}$$

Equation (23) properly describes the simulated energy distribution in the case of CVI conditions, $R_0 < R_0^{(I)}$ [Fig. 7(a)], in the intermediate case of $R_0 \approx R_0^{(I)}$ [Fig. 7(b)], as well as in the "cold" nanoplasma case, $R_0 \gg R_0^{(I)}$ [Fig. 7(c)].

V. CONCLUDING REMARKS

The present study of cluster Coulomb explosion extended the arsenal of theoretical models to treat the non-CVI domain. The benchmark data for the applicability of the theoretical models involve computational results based on molecular dynamics simulations. It would be very useful to apply experimental data for this purpose, however, these are scarce, being available only for deuterium clusters at very high intensities of I_M=2×10^{18} W cm^{-2} [14]. For these intensities, the outer ionization of a $(D_2)_{n/2}$ cluster is complete on a time scale of t_{oi}=25 fs for n=8007 (R_0=34 Å) [27], the nanoplasma is transient and the Coulomb explosion corresponds to the CVI domain. Our previous analysis [27] showed that for the energetics of Coulomb explosion of $(D_2)_{n/2}$ clusters ($E_{\rm av}$=5–7 keV at I_M=2×10^{18} W cm^{-2}) the experimental data in this CVI domain [14] can be accounted for by the simulation results for these clusters with R_0=51–60 Å, which exceed by 10%–25% the experimental estimate of R_0=45 Å [27]. This agreement between experiments and simulations in the CVI domain is quite satisfactory, in view of the uncertainties in the experimental estimates of the cluster radii and their size distribution [1,14,20,45]. The maximal ion energy E_M is much more strongly affected than the average energy $E_{\rm av}$ by the size spread of the clusters [14,45]. Consequently, the ion energy distribution $P(E)$ produced by the ensemble of size distributed clusters is expected to be different from the single cluster energy distribution, Eq. (23), which precludes the comparison of our theoretical energy distributions with the experimental results. The effect of cluster size distributions on the product ion energetics will be considered in a forthcoming paper [46]. In view of the absence of experimental data for the non-CVI regime, simulation results must be confronted with the predictions of the "cold" nanoplasma model.

Two comments regarding the applicability of the simulation results for the description of the nanoplasma (at all I_M values) and of the "cold" nanoplasma model (in the intensity range of I_M=10^{15}–10^{16} W cm^{-2}) will be in order. First, we

examine the validity conditions for the molecular dynamics scheme to describe the nanoplasma (Sec. I). It appears that the condition for distinguishability of identical particles [43] is well obeyed for $I_M \geqslant 10^{15}$ W cm^{-2}. The validity condition for the localization of the wave packet [42] requires high ($\in \gtrsim 100$ eV) nanoplasma electron energies. Our simulations for $(D_2)_{n/2}$ ($n=16\,000$) clusters resulted in $\in = 50-100$ eV for $I_M = 10^{15}$ W cm^{-2}, $\in = 0.2-2$ keV for $I_M = 10^{16}$ W cm^{-2}, and $\in = 1-4$ keV for $I_M = 10^{17}$ W cm^{-2}. Accordingly, the localization of the wave packet is insured for $I_M > 10^{15}$ W cm^{-2}. Our use of molecular dynamics for the nanoplasma electrons at $I_M = 10^{15}$ W cm^{-2} touches on the lower limit for the intensity domain, which is physically acceptable for this scheme. Second, we consider the issue of light absorption by the nanoplasma. In the non-CVI domain, where the nanoplasma is persistent [36], one may consider the enhancement of light absorption by resonance effects, which generate nanoplasma oscillations [1,3,47–50]. The frequency of the linear oscillations for a thermally equilibrated and uniform nanoplasma is [1,36,43,45] $\omega_p = (4\pi e^2 \rho_p / 3m)^{1/2}$. The initial electron density ρ_p in the persistent nanoplasma prior to Coulomb explosion is equal to the ion density, i.e., $\rho_p = \rho$, so that $\rho_p = 0.05$ Å^{-3} for $(D_2)_{n/2}$ clusters. The nanoplasma energy is then $\hbar\omega_p = 4.8$ eV. This value of $\hbar\omega_p$ is significantly larger than the photon energy $\hbar\omega = 1.44$ eV used in our simulations. It was suggested that the resonance conditions may be realized in the course of Coulomb explosion, when ρ_p decreases with cluster expansion [50]. Our simulations reveal that the persistent nanoplasma maintains the initial spatial configuration of the electron cloud, which does not expand uniformly throughout the nuclear framework of the Coulomb exploding cluster. Furthermore our simulations, which take into account all the interactions which determine the electron trajectories in the coupled cluster-laser system, are expected to describe the nanoplasma oscillations. Our simulation results for the dynamics of nanoplasma electrons in the course of Coulomb explosion do not reveal any steep temporal increase of the electron energy, which could be interpreted as a resonance generation of nanoplasma oscillations, precluding the possibility of such excitations. In the CVI domain ($R_0 < R_0^{(I)}$) and at the onset of the non-CVI domain ($R_0 \sim R_0^{(I)}$), the lack of distinct resonance energy absorption by cluster electrons can be explained by asserting that these electrons form highly nonequilibrium and spatially nonuniform systems [36] whose behavior cannot be described in terms of the plasma oscillation theory.

The present study focuses on the non-CVI domain of cluster Coulomb explosion where the persistent nanoplasma within the cluster dominates nuclear dynamics. A classification of the two regions, the CVI and the non-CVI "cold" nanoplasma domains in the R_0 vs I_M (fixed τ) plane, is summarized in Fig. 8. The gross effects of the persistent nanoplasma on the energetics of Coulomb explosion are manifested by deviations of E_{av} and E_M from the CVI-type cluster size scaling equation, with the energies being systematically lower in the non-CVI regime than predicted for the CVI regime, Eqs. (2) and (3). The transition from the CVI domain ($R_0 < R_0^{(I)}$) to the non-CVI domain ($R_0 > R_0^{(I)}$) is characterized by the border cluster radius $R_0^{(I)}$, which is dependent on the

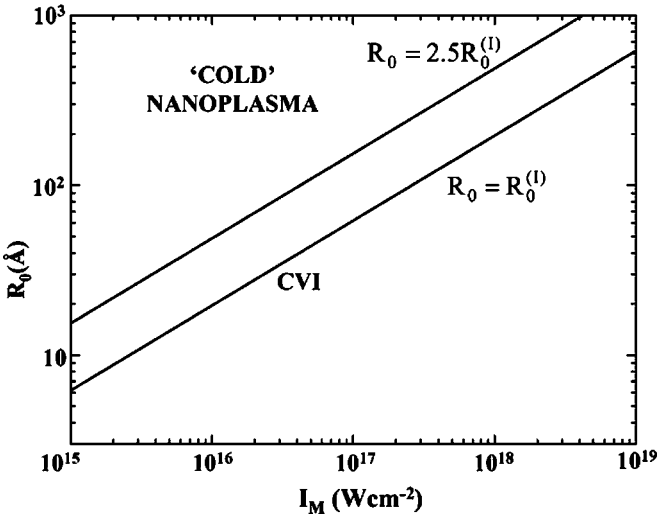

FIG. 8. A schematic classification of the CVI and non-CVI domains for Coulomb explosion, relating electron and nuclear dynamics of $(D_2)_{n/2}$ clusters subjected to Gaussian laser pulses ($\tau = 25$ fs) in the intensity domain $I_M = 10^{15}-10^{18}$ W cm^{-2}. The area below the lower line $R_0 = R_0^{(I)}$ corresponds to the CVI domain, while the area above the upper line $R_0 = 2.5R_0^{(I)}$ corresponds to the "cold" non-CVI domain, where the nanoplasma model is applicable. The dependence of $R_0^{(I)}$ on I_M was obtained from Eq. (8), with $A = 1.95 \times 10^{-7}$ Å/(W cm^{-2})$^{1/2}$.

laser parameters (peak intensity and pulse duration), and on the chemical and physical nature (structure, electronic structure, and ionization energies) of the cluster. On the basis of our simulations we assert that the non-CVI "cold" nanoplasma domain prevails for $R_0 > (2.0-2.5)R_0^{(I)}$. We note in passing that border radii marking the upper limits for the $E_{\mathrm{av}} \propto R_0^2$ energy dependence were previously introduced (as $r_{\max}$ values) in the Coulomb explosion model of Parks *et al.* [20]. However, the physical meaning of these two parameters, $R_0^{(I)}$ introduced herein and $r_{\max}$ [20], is markedly different. The $r_{\max}$ radius of Parks *et al.* [20] sets an unphysical upper limit for Coulomb explosion (i.e., $E_{\mathrm{av}} = 0$ for $R_0 > r_{\max}$), whereas the $R_0^{(I)}$ radius of Eq. (8) and Fig. 3 manifests the onset of the cluster size domain, where a slowing down of the linear increase of E_{av} with increasing $(R_0)^2$ is exhibited. Furthermore, the work of Parks *et al.* [20] did not address the effect of the persistent nanoplasma on the Coulomb explosion energetics, which constitutes a central ingredient of our work.

In general, the CVI regime prevails over a broad cluster size domain in the laser intensity range $I_M \gtrsim 10^{17}$ W cm^{-2}, while for lower intensities, when the onset of the non-CVI sets in for $R_0 > R_0^{(I)}$, the CVI regime is realized only for small clusters [e.g., for $(D_2)_{n/2}$ at $I_M = 10^{15}$ W cm^{-2}, $R_0^{(I)} = 6.2$ Å for $\tau = 25$ fs, and $R_0^{(I)} = 9.5$ Å for $\tau = 50$ fs]. So, in the intensity domain of $I_M \lesssim 10^{16}$ W cm^{-2} the non-CVI domain dominates. In view of the ubiquity of recent experimental studies of laser-cluster interaction in the intensity domain of $I_M = 10^{14}-10^{16}$ W cm^{-2} [9,12,13,15], the present study of the energetics of Coulomb explosion in the non-CVI regime is of considerable interest.

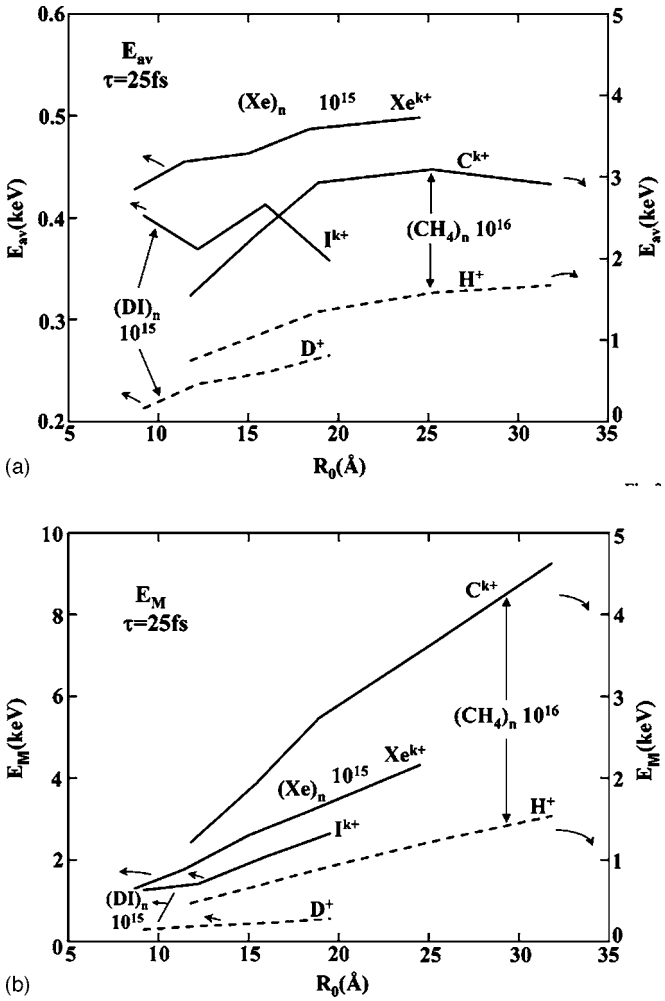

FIG. 9. Cluster size dependence of the energies of the product ions from Coulomb explosion of $(Xe)_n$, $(CH_4)_n$, and $(DI)_n$ clusters in the non-CVI domain. Laser pulse width $\tau=25$ fs. Laser peak intensities $I_M=10^{15}$ W cm^{-2} for $(Xe)_n$ and $(DI)_n$ clusters, and $I_M=10^{16}$ W cm^{-2} for $(CH_4)_n$ clusters. (a) Average ion energies E_{av} vs R_0, which manifest a weak cluster size dependence. (b) Maximal ion energies E_M vs R_0, which manifest a near-linear increase with increasing R_0.

We have studied the energetics of the non-CVI regime by molecular dynamics simulations of electrons and ions, which were fit by semiempirical equations for E_{av}, for E_M, and for the distribution of the kinetic energies. This fitting procedure, which is determined by the border cluster radius $R_0^{(I)}$, results in an asymptotic cluster size dependence (or independence) for E_{av} and E_M (for $R_0 \gg R_0^{(I)}$). This can qualitatively be described in terms of a "cold" nanoplasma model, and is based on a lychee type structure of the nanoplasma charge within the cluster. It is important to note that the results of the present study are of broad applicability, being also relevant for Coulomb explosion of other elemental and molecular clusters. The saturation of E_{av} and of the linear E_M vs R_0 dependence at $R_0 \gg R_0^{(I)}$ found herein for deuterium clusters were also found from molecular dynamics simulations for other clusters, e.g., atomic Xe_n [40,51] [Figs. 9(a) and 9(b)] and molecular heteroclusters, i.e., $(CH_4)_n$ [28] [Figs. 9(a) and 9(b)], and $(ID)_n$ [51] [Figs. 9(a) and 9(b)]. In the case of Xe_n clusters, the "cold" nanoplasma behavior is manifested by saturation of E_{av} [Fig. 9(a)] and by the near linear increase of E_M [Fig. 9(b)] at $I_M=10^{15}$ W cm^{-2} over the entire domain of the cluster radii studied by us. The same behavior is exhibited for light (H^+) and heavy (C^{k+}, $k=3-4$) ions from methane clusters [28] at $R_0>20$ Å at $I_M=10^{16}$ W cm^{-2} [Figs. 9(a) and 9(b)], and for light (D^+) and heavy (I^{k+}, $k=4-5$) ions from $(ID)_n$ clusters [51] at $R_0>12$ Å at $I_M=10^{15}$ W cm^{-2} [Figs. 9(a) and 9(b)]. In view of the cluster size dependence of the ionization level of the heavy ions [28,40,51], the near independence of E_{av} on R_0 reveals slight deviations from saturation for the heavy ions. The average energies of the heavy ions in the "cold" nanoplasma domain decrease slightly with increasing R_0, manifesting faint maxima at the beginning of this domain [Fig. 9(b)] [51].

The fitting equations advanced and evaluated for the deuteron energetics and bimodal energy distribution, Eqs. (6), (7), (23), and (26), allow us to describe the energetics of deuterons produced by Coulomb explosion of a single $(D_2)_{n/2}$ cluster for an arbitrary cluster size, laser pulse intensity and laser pulse duration. These relations can be generalized for Coulomb explosion of deuterium containing heteroclusters. These fitting equations are very useful when an ensemble of differently sized clusters is subjected to nonuniform laser radiation. In forthcoming papers we shall apply these equations to treat light absorption by clusters [52] and to study the effect of light absorption and cluster size distribution on the *dd* nuclear fusion [46] driven by Coulomb explosion of deuterium clusters.

ACKNOWLEDGMENTS

This research was supported by the Deutsche Forschungsgemeinschaft (SFB 450) on Analysis and Control of Ultrafast Photoinduced Reactions, and by the German-Israeli James Franck program on laser-matter interaction.

[1] T. Ditmire, T. Donnely, A. M. Rubenchik, R. W. Falcone, and M. D. Perry, Phys. Rev. A **53**, 3379 (1996).
[2] T. Ditmire, J. W. G. Tisch, E. Springate, M. B. Mason, N. Hay, R. A. Smith, J. Marangos, and M. H. R. Hutchinson, Nature (London) **386**, 54 (1997).
[3] T. Ditmire, E. Springate, J. W. G. Tisch, Y. L. Shao, M. B. Mason, N. Hay, J. P. Marangos, and M. H. R. Hutchinson, Phys. Rev. A **57**, 369 (1998).
[4] J. V. Ford, O. Zhong, L. Poth, and A. W. Castleman, Jr., J. Chem. Phys. **110**, 6257 (1999).
[5] M. Lezius, V. Blanchet, D. M. Rayner, D. M. Villeneuve, A. Stolov, and M. Yu. Ivanov, Phys. Rev. Lett. **86**, 51 (2001).
[6] E. Springate, N. Hay, J. W. G. Tisch, M. B. Mason, T. Ditmire, M. H. R. Hutchinson, and J. P. Marangos, Phys. Rev. A **61**,

063201 (2000).
[7] J. Zweiback, R. A. Smith, T. E. Cowan, G. Hays, K. B. Wharton, V. P. Yanovsky, and T. Ditmire, Phys. Rev. Lett. **84**, 2634 (2000).
[8] S. Teuber, T. Döppner, T. Fennel, J. Tiggesbäumker, and K. H. Meiwes-Broer, Eur. Phys. J. D **16**, 59 (2001).
[9] D. A. Card, E. S. Wisniewski, D. E. Folmer, and A. W. Castleman, Jr., J. Chem. Phys. **116**, 3554 (2002).
[10] G. Grillon, Ph. Balcou, J.-P. Chambaret, D. Hulin, J. Martino, S. Moustaizis, L. Notebaert, M. Pittman, Th. Pussieux, A. Rousse, J-Ph. Rousseau, S. Sebban, O. Sublemontier, and M. Schmidt, Phys. Rev. Lett. **89**, 065005 (2002).
[11] J. Schulz, H. Habnitz, T. Laarmann, S. Gürtler, W. Laasch, A. Swiderski, Th. Möller, and A. A. B. de Castro, Nucl. Instrum. Methods Phys. Res. A **507**, 572 (2003).
[12] V. Kumarappan, M. Krishnamurthy, and D. Mathur, Phys. Rev. A **67**, 063207 (2003).
[13] M. Krishnamurthy, D. Mathur, and V. Kumarappan, Phys. Rev. A **69**, 033202 (2004).
[14] K. W. Madison, P. K. Patel, D. Price, A. Edens, M. Allen, T. E. Cowan, J. Zweiback, and T. Ditmire, Phys. Plasmas **11**, 270 (2004).
[15] T. Laarman, A. R. B. De Castro, P. Gürtler, W. Laasch, J. Schulz, H. Wabnitz, and T. Möller, Phys. Rev. Lett. **92**, 143401 (2004).
[16] T. Ditmire, Phys. Rev. A **57**, R4094 (1998).
[17] I. Last and J. Jortner, Phys. Rev. A **62**, 013201 (2000).
[18] K. Ishikava and T. Blenski, Phys. Rev. A **62**, 063204 (2000).
[19] J. Liu, R. Li, P. Zhu, Zh. Xu, and J. Liu, Phys. Rev. A **64**, 033426 (2001).
[20] P. B. Parks, T. E. Cowan, R. B. Stephens, and E. M. Campbell, Phys. Rev. A **63**, 063203 (2001).
[21] I. Last and J. Jortner, Phys. Rev. Lett. **87**, 033401 (2001).
[22] I. Last and J. Jortner, Phys. Rev. A **64**, 063201 (2001).
[23] I. Last and J. Jortner, J. Phys. Chem. A **106**, 10877 (2002).
[24] V. P. Krainov and M. B. Smirnov, Phys. Rep. **370**, 237 (2002).
[25] Ch. Siedschlag and J. M. Rost, Phys. Rev. A **67**, 013404 (2003).
[26] Z. Jurek, G. Faigel, and M. Tegze, Eur. Phys. J. D **29**, 217 (2004).
[27] I. Last and J. Jortner, J. Chem. Phys. **121**, 3030 (2004).
[28] I. Last and J. Jortner, J. Chem. Phys. **121**, 8329 (2004).
[29] D. Bauer and A. Macchi, Phys. Rev. A **68**, 033201 (2003).
[30] R. Santra and Ch. H. Greene, Phys. Rev. Lett. **91**, 233401 (2003).
[31] A. H. Zewail, *Femtochemistry: Ultrafast Dynamics of the Chemical Bond* (World Scientific, Singapore, 1994).
[32] *Femtosecond Chemistry*, edited by J. Manz and W. Wöste (VCH, Weinheim, 1995).
[33] *Femtochemistry: Ultrafast Chemical and Physical Processes in Molecular Systems*, edited by M. Chergui (World Scientific, Singapore, 1996).
[34] *Femtochemistry and Femtobiology*, edited by V. Söndstrom, Nobel Symposium 101 (Imperial College Press, London, 1997).
[35] J. Jortner, Proc. R. Soc. London, Ser. A **356**, 477 (1998).
[36] I. Last and J. Jortner, J. Chem. Phys. **120**, 1348 (2004).
[37] J. Daligault and C. Guet, Phys. Rev. A **64**, 043203 (2001).
[38] T. Fennel, C. F. Bertsch, and K.-M. Meiwes-Broer, Eur. Phys. J. D **29**, 367 (2004).
[39] I. Last and J. Jortner, Phys. Rev. A **62**, 013201 (2000).
[40] I. Last and J. Jortner, J. Chem. Phys. **120**, 1336 (2004).
[41] Y. Fukuda, K. Yamakawa, Y. Akahane, M. Aoyama, N. Inoue, H. Ueda, and Y. Kishimoto, Phys. Rev. A **67**, 061201(R) (2003).
[42] M. P. Allen and D. J. Tildesley, *Computer Simulations of Liquids* (Clarendon, Oxford Science, Oxford, 1992).
[43] R. P. Feynman and A. R. Hibbs, *Quantum Mechanics and Path Integrals* (McGraw-Hill, New York, 1965).
[44] In our previous papers [27,28] $R_0^{(I)}$ was denoted by $(R_0)_I$.
[45] K. J. Mendham, N. Hay, M. B. Mason, J. W. G. Tisch, and J. P. Marangos, Phys. Rev. A **64**, 055201 (2001).
[46] I. Last and J. Jortner (unpublished).
[47] U. Saalmann and J.-M. Rost, Phys. Rev. Lett. **91**, 223401 (2003).
[48] Ch. Siedschlag and J.-M. Rost, Phys. Rev. A **71**, 031401 (2005).
[49] S. V. Fomichev, S. V. Popruzhenko, D. F. Zaretsky, and W. Becker, J. Phys. B **36**, 3817 (2003).
[50] S. V. Fomichev, D. F. Zaretsky, D. Bauer, and W. Becker, Phys. Rev. A **71**, 013201 (2005).
[51] A. Heidenreich, I. Last, and J. Jortner (unpublished).
[52] I. Last and J. Jortner, Attenuation of Ultraintense Laser Radiation in an Assembly of Molecular Clusters (to be published).